Imaging Macrophage and Hematopoietic Progenitor Proliferation in Atherosclerosis

HHS Public Access

Author manuscript

Circ Res. Author manuscript; available in PMC 2016 October 23.

Published in final edited form as:

Circ Res. 2015 October 23; 117(10): 835–845. doi:10.1161/CIRCRESAHA.115.307024.

Imaging Macrophage and Hematopoietic Progenitor Proliferation in Atherosclerosis

Yu-Xiang Ye[1], **Claudia Calcagno**[2], **Tina Binderup**[3], **Gabriel Courties**[1], **Edmund J. Keliher**[1], **Gregory R. Wojtkiewicz**[1], **Yoshiko Iwamoto**[1], **Jun Tang**[2], **Carlos Pérez-Medina**[2], **Venkatesh Mani**[2], **Seigo Ishino**[2], **Camilla Bardram Johnbeck**[3], **Ulrich Knigge**[4], **Zahi A. Fayad**[2], **Peter Libby**[5], **Ralph Weissleder**[1,6], **Ahmed Tawakol**[7], **Shipra Dubey**[8], **Anthony P. Belanger**[8], **Marcelo F. Di Carli**[5,8], **Filip K. Swirski**[1], **Andreas Kjaer**[3], **Willem J.M. Mulder**[2,9], and **Matthias Nahrendorf**[1]

[1]Center for Systems Biology, Massachusetts General Hospital and Harvard Medical School, Simches Research Building, 185 Cambridge St., Boston, MA 02114, USA [2]Translational and Molecular Imaging Institute, Department of Radiology, Icahn School of Medicine at Mount Sinai, One Gustave L. Levy Place, NY 10029, New York, United States [3]Dept. of Clinical Physiology, Nuclear Medicine & PET and Cluster for Molecular Imaging, KF-4012, Rigshospitalet, National University Hospital & University of Copenhagen, Blegdamsvej 9, DK-2100 Copenhagen, Denmark [4]Departments of Clinical Endocrinology PE and Surgery C, Rigshospitalet, National University Hospital & University of Copenhagen, Blegdamsvej 9, DK-2100 Copenhagen, Denmark [5]Cardiovascular Division, Department of Medicine, Brigham and Women's Hospital, Boston, MA, USA [6]Department of Systems Biology, Harvard Medical School, Boston, MA, USA [7]Division of Cardiology, Massachusetts General Hospital and Harvard Medical School, Boston, MA, USA [8]Division of Nuclear Medicine and Molecular Imaging, Department of Radiology, Brigham and Women's Hospital, Harvard Medical School, Boston MA, USA [9]Department of Vascular Medicine, Academic Medical Center, Amsterdam, 1105 AZ, The Netherlands

Abstract

Rationale—Local plaque macrophage proliferation and monocyte production in hematopoietic organs promote progression of atherosclerosis. Therefore, non-invasive imaging of proliferation could serve as a biomarker and monitor therapeutic intervention.

Objective—To explore ^{18}F-fluorothymidine (^{18}F-FLT) PET-CT imaging of cell proliferation in atherosclerosis.

Address correspondence to: Matthias Nahrendorf, Center for Systems Biology, 185 Cambridge Street, Boston, MA 02114, Tel: (617) 643-0500, Fax: (617) 643-6133, mnahrendorf@mgh.harvard.edu.

DISCLOSURES

None.

Subject terms:

Nuclear cardiology and PET

Imaging

Mechanisms

Pathophysiology

Methods and Results—^{18}F-FLT PET-CT was performed in mice, rabbits and humans with atherosclerosis. In ApoE$^{-/-}$ mice, increased ^{18}F-FLT signal was observed in atherosclerotic lesions, spleen and bone marrow (SUV wild-type versus ApoE$^{-/-}$ mice, 0.05±0.01 versus 0.17±0.01, P<0.05 in aorta; 0.13±0.01 versus 0.28±0.02, P<0.05 in bone marrow; 0.06±0.01 versus 0.22±0.01, P<0.05 in spleen), corroborated by ex vivo scintillation counting and autoradiography. Flow cytometry confirmed significantly higher proliferation of macrophages in aortic lesions and hematopoietic stem and progenitor cells in the spleen and bone marrow in these mice. In addition, ^{18}F-FLT plaque signal correlated with the duration of high cholesterol diet (r^2=0.33, p<0.05). Aortic ^{18}F-FLT uptake was reduced when cell proliferation was suppressed with 5-FU in ApoE$^{-/-}$ mice (p<0.05). In rabbits, inflamed atherosclerotic vasculature with the highest ^{18}F-fluorodeoxyglucose uptake enriched ^{18}F-FLT. In patients with atherosclerosis, ^{18}F-FLT signal significantly increased in the inflamed carotid artery and in the aorta.

Conclusions—^{18}F-FLT PET imaging may serve as an imaging biomarker for cell proliferation in plaque and hematopoietic activity in individuals with atherosclerosis.

Keywords

Atherosclerosis; ^{18}F-Fluorothymidine; cardiac positron emission tomography; macrophage; inflammation; proliferation; imaging

INTRODUCTION

Inflammatory monocytes and macrophages are innate immune cells that promote the growth and complication of atherosclerotic lesions. Once recruited to the arterial wall, mononuclear phagocytes can ingest lipoproteins. Often, the cells produce pro-inflammatory mediators and differentiate into foam cells. Activated macrophages also elaborate proteases that weaken the plaque's extracellular matrix[1, 2]. In early-stage atherosclerosis in mice, most plaque macrophages are direct progeny of recruited blood monocytes that originate in the bone marrow and spleen. In advanced disease, monocyte-derived macrophages proliferate locally, a process that contributes dominantly to the cell population in mature plaques[3]. Hence, in early and in late disease stages, cellular proliferation pivotally promotes expansion of both the systemic and local myeloid cell pools. By extension, proliferation likely also drives disease progression. Hematopoietic cell proliferation, either remote in bone marrow and spleen or locally in plaque, may thus represent a therapeutic target.

Commonly, we rely on ex vivo cell cycle analysis to measure cellular proliferation. These assays have limited use for assessing proliferative tissue activity in patients with atherosclerosis because the tissues of interest are not readily available for biopsy. With few exceptions, we are currently limited to investigating circulating leukocytes. However, these cells do not proliferate, and monocyte numbers in blood may not faithfully reflect proliferation in plaque or hematopoietic organs. In a hypothetical scenario, plaque macrophage proliferation may be high despite normal blood monocyte levels, resulting in inflamed vascular lesions that are prone to complications. An imaging biomarker that reports on proliferating cells would expand diagnostic capabilities to disease-relevant tissues and aid development of emerging cardiovascular immuno-modulatory drugs.

Imaging of cancer cells has explored the use of such a biomarker[4]. ^{18}F-fluoro-3′-deoxy-3′-L-fluorothymidine (^{18}F-FLT), a PET isotope-labeled thymidine analog, enriches in proliferating cells. Phosphorylation traps the agent intracellularly[5]. Thymine is one of the four bases needed for DNA replication that occurs before cell division. The small molecule PET agent ^{18}F-FLT has undergone clinical exploration for assessing proliferation, and its retention correlates with the histological cell cycle marker Ki67 in tumor cells, especially in brain, lung and breast cancer[6]. In oncology, ^{18}F-FLT has emerged as a promising strategy to monitor treatment response for some cancers that rely more on the DNA salvage pathway than on de novo thymidine synthesis[5, 7, 8]. The comparable proliferative rates of cancer cells and plaque macrophages, and previous reports of ^{18}F-FLT uptake into hematopoietic tissues[5, 9, 10] led us to hypothesize that this agent could prove useful for imaging hematopoietic cells in cardiovascular disease. The frequent use of the thymidine analog BrdU, an established tool in hematology to measure leukocyte and progenitor proliferation, further suggested that the thymidine analog ^{18}F-FLT may report on macrophage proliferation.

Here we show that atherosclerotic plaques in atherosclerotic ApoE$^{-/-}$ mice, rabbits and patients accumulate ^{18}F-FLT. In accordance with the recently reported increase of macrophage proliferation in mature atherosclerotic lesions[3], aortic ^{18}F-FLT retention correlates with the duration of an atherogenic diet in mice and with the Framingham Risk Score in patients. Macrophage-rich plaques with high ^{18}F-FDG signal show the highest ^{18}F-FLT uptake in atherosclerotic rabbit aortae. Hematopoietic organ ^{18}F-FLT uptake associates with hematopoietic activity: it increases in mice with atherosclerosis and after exposure to the Toll-like receptor (TLR) ligand lipopolysaccharide (LPS), and decreases after injection of fluorouracil (5-FU), an antimetabolite drug that kills proliferating cancer cells and cycling hematopoietic stem and progenitor cells (HSPCs).

METHODS

A detailed method section is available in the Online Data Supplement.

Mice

Female apolipoprotein E knock out (ApoE$^{-/-}$) and wild-type C57BL/6 mice (10–12 weeks old) were purchased from Jackson Laboratories. Atherosclerosis was induced by feeding high cholesterol diet to ApoE$^{-/-}$ mice ranging from 10 to 28 weeks. In wild-type mice, modulation of hematopoietic progenitor cell proliferation in bone marrow and the spleen were induced by injecting lipopolysaccharide (LPS, 10μg/mouse i.p. on three and one days before imaging) and fluorouracil (5-FU, 150μg/g i.p. 12 hours before imaging). To investigate whether the ^{18}F-FLT uptake in atherosclerosis reflects cell proliferation, an additional cohort of ApoE$^{-/-}$ mice was treated with 5-FU at the dose of 150μg/g i.p. 12 and 4 hours before injecting ^{18}F-FLT. For cell cycling analysis by flow cytometry, bromodeoxyuridine (BrdU, DB Biosciences), an antibody-recognizable analog of thymidine, was injected i.p. in these ApoE$^{-/-}$ mice immediately after ^{18}F-FLT injection. All procedures in mice were approved by the Institutional Animal Care and Use Committee Subcommittee on Research Animal Care, Massachusetts General Hospital, Charlestown, MA.

Rabbits

Atherosclerosis was induced in 4 male New Zealand White (NZW) rabbits by a combination of high-cholesterol diet and double balloon injury of the abdominal aorta[11]. Rabbits were imaged 6 months after diet initiation. Four control rabbits received normal diet. All procedures in rabbits were approved by the IACUC at Mount Sinai Hospital, New York City, NY.

Small animal positron emission tomography (PET)-computed tomography (CT) imaging and image analysis

^{18}F-FLT was injected via tail vein 120 min before in vivo imaging with an average dose of 22.44±1.07MBq. This dose and imaging time point were chosen based on published biodistribution data and because mice have high circulating thymidine levels that compete with the PET agent for uptake into proliferating cells[7]. Mice were imaged with an Inveon small-animal PET-CT scanner (Siemens Medical Solutions, Inc., Malvern, Pennsylvania). CT was performed prior to PET, acquiring 360 cone beam projections (source power 80 keV and current 500 μA). During CT acquisition, iodine contrast was infused via the tail vein at a rate of 35μl/minute. For quantitative analysis, 1–3 regions of interest (ROIs) were drawn manually in the aortic root, the spleen and the spine of each animal, guided by CT images. After in vivo imaging, mice were sacrificed and the direct γ counting was performed on the aortic root, the spleen and a femur. The data are presented as percent injected dose per gram of tissue (%IDGT).

Rabbit imaging

Animals were subjected to high-resolution 3 dimensional T2-weighted magnetic resonance imaging (MRI) with a 7-tesla scanner (Magnetom 7T, Siemens Healthcare, Erlangen, Germany). To establish ^{18}F-FLT's pharmacokinetics, animals were injected with ~111MBq and blood was drawn at 2, 5, 15, 30, 60, 120 and 240 min. Radioactivity was measured by a Wizard 2470 Perkin Elmer automatic gamma counter. Values were calculated as %IDGT. All 8 rabbits (average weight 3.47 ± 0.37 Kg) underwent two PET/CT scans, on 2 different days. The first PET/CT was performed after injection of ^{18}F-FDG, while the second PET/CT was performed after the injection of ^{18}F-FLT. For both imaging sessions rabbits were fasted for 4 hours before the isotope injection (water was provided at libitum). Before injection rabbits were appropriately restrained, and the isotope was injected through a catheter placed in a marginal ear vein. The average injected dose of FDG was 190.3 ± 9.9 MBq (55.2 ± 5.0 MBq/Kg), while the average injected dose of FLT was 199.2 ± 29.1 MBq (57.5 ± 8.0 MBq/Kg). Rabbits were imaged approximately 200 minutes after isotope injection (^{18}F-FDG: 197.5 ± 5.50 minutes; ^{18}F-FLT: 198.9 ± 10.5 minutes). Approximately 15 minutes before imaging, rabbits were anesthetized using an injection of ketamine (35mg/kg) and xylazine (5mg/kg), and the bladder was emptied. Anesthesia was maintained during imaging using 1% isofluorane breathing anesthesia. PET/CT was performed using a clinical scanner (Siemens Biograph mCT, PET/CT, Siemens, Erlangen, Germany), in 3D mode, using one bed position, for 60 minutes. Images were acquired from the thoracic aorta, down to the iliac bifurcation. A non contrast enhanced CT was also performed for attenuation correction of the PET images, and to identify the aorta during image analysis.

Human FDG-PET/CT and FLT-PET/CT

Twenty patients with paired FLT-PET/CT and FDG-PET/CT scans performed between December 2011 and March 2013 were retrospectively included. Ten patients with high risk of cardiovascular disease (atherosclerotic group) and 10 patients with low risk (control group) were enrolled based on their Framingham Score (Table 1). The study was performed in accordance with the Helsinki Declaration and approved by the regional scientific ethical committee (H-3-2011-092). All patients were diagnosed with neuroendocrine tumors and written informed consent was obtained from all participants. Patients underwent an FDG-PET/CT and an FLT-PET/CT within 2 weeks of each other performed on a Siemens Biograph 40 or 64 PET/CT scanner (Siemens Medical Systems, Erlangen, Germany). Patients were instructed to fast at least 6 hours prior to tracer injection and static images were acquired 1 hour post-injection of either ^{18}F-FDG or ^{18}F-FLT. Reconstructed images were analyzed using the OsiriX Lite open-source software (Pixmeo). Image analysis was done in a blinded fashion on anonymized scans. Tracer uptake was quantified as maximum and mean Standardized Uptake Values (SUV max and SUV mean). ROIs were drawn on all slices of the ascending aorta and at least 10 consecutive slices of the carotid artery. Averaged SUV max and SUV mean were then calculated for each patient in the 2 target regions based on SUV max and SUV mean values from all ROIs in the respective region. To correlate the uptake of ^{18}F-FDG and ^{18}F-FLT on a sub-regional level, matched slices of ^{18}F-FDG and ^{18}F-FLT scans were analyzed side-by-side in the ascending aorta.

RESULTS

Arterial uptake of ^{18}F-FLT increases in ApoE$^{-/-}$ mice

We began by exploring the uptake of ^{18}F-FLT in the thoracic aorta of ApoE$^{-/-}$ mice that consumed a high fat diet. In these mice, the aortic root harbors plaques inhabited by proliferating macrophages. ApoE$^{-/-}$ but not wild-type mice had areas of increased PET signal that colocalized with the aortic root and the ascending aorta on CT angiography (Fig. 1A). The PET derived SUV measured in the aortic root in ApoE$^{-/-}$ mice significantly exceeded that in wild-type mice (wild-type controls versus ApoE$^{-/-}$ mice, 0.053 ± 0.010 versus 0.169 ± 0.013, $P<0.05$) (Fig. 1B). We further observed signal in the thoracic vertebrae and the sternum in both cohorts, a finding that stimulated further exploration. Ex vivo data obtained by scintillation counting (%IDGT, wild-type controls versus ApoE$^{-/-}$ mice, 0.214 ± 0.015 versus 0.376 ± 0.037, $P<0.05$) (Fig. 1C) and autoradiography (Fig. 1D) confirmed higher activity in the aortae excised from ApoE$^{-/-}$ mice, and peak signal colocalized with Oil Red O stained atherosclerotic lesions. As reported previously, the aortic root contained numerous Ki67$^+$ CD68$^+$ macrophages (Fig. 1E)[3]. Macrophages contributed 73.5 ± 2.8% of all proliferating Ki67$^+$ cells in the aortic wall. We found significantly less proliferating endothelial cells, smooth muscle cells and T lymphocytes in the atherosclerotic aortic root (Fig. 1E,F). The fraction of proliferating macrophages was quantified in digested whole aortae by flow cytometric analysis. Significantly more macrophages were in the active S/G2/M phases of the cell cycle in aortae harvested from ApoE$^{-/-}$ mice (Fig. 1G, H). Previously we had described that local macrophage proliferation increases in mature atherosclerotic lesions[3]. In line with these data, we found a positive correlation between scintillation counts in aortae of mice injected with ^{18}F-FLT and the duration of the

atherogenic diet (Fig. 1I). In ApoE$^{-/-}$ mice that received 5-FU, which reduces cell proliferation[3], uptake of ^{18}F-FLT in the aortic root was reduced (Fig. 2A–C), in parallel with reduced BrdU^{+} macrophages detected by flow cytometry (Fig. 2D,E). Of note, ^{18}F-FLT and BrdU are both thymidine analogs and were injected at the same time. These data suggest that ^{18}F-FLT signal in atherosclerotic mouse aortae mostly reflects local proliferation of macrophages, but other cells such as endothelial or smooth muscle cells may also contribute to the PET signal to a smaller degree.

^{18}F-FLT signal in hematopoietic organs of ApoE$^{-/-}$ mice

The thymidine analog ^{18}F-FLT enriches in organs with high proliferative rates, including the hematopoietic bone marrow[5]. Intrigued by our observation of high PET signal in the sternum and vertebrae, and because the hematopoietic system supplies monocytes to inflamed atherosclerotic plaque, we systematically compared ^{18}F-FLT uptake in the bone marrow and spleen of ApoE$^{-/-}$ mice to wild-type controls (Fig. 3A). In vivo SUV in bone marrow rose in mice with atherosclerosis (wild-type controls versus ApoE$^{-/-}$ mice, 0.132 ± 0.013 versus 0.276 ± 0.020, P<0.05) (Fig. 3B), as did activity detected by ex vivo scintillation counting (%IDGT of the femur, wild-type controls versus ApoE$^{-/-}$ mice, 0.735 ± 0.053 versus 1.261 ± 0.114, P<0.05) (Fig. 3C). These observations could result from higher thymidine uptake, DNA synthesis and proliferation of HSPC. Indeed, flow cytometric analysis paralleled the in vivo PET data, as more Lineage^{-} c-Kit^{+} Sca-1^{+} (LSK) progenitor cells were in the S/G2/M phase of the cell cycle (Fig. 3D, E). Examination of the spleen yielded a similar pattern: both in vivo PET signal (SUV, wild-type controls versus ApoE$^{-/-}$ mice, 0.059 ± 0.007 versus 0.224 ± 0.013, P<0.05) (Fig. 3F, G) and ex vivo scintillation counting of the organ (%IDGT, wild-type controls versus ApoE$^{-/-}$ mice, 0.455 ± 0.065 versus 1.345 ± 0.134, P<0.05) (Fig. 3H) revealed higher ^{18}F-FLT uptake. As in the marrow, the higher tracer uptake paralleled increased cycling of LSK in the spleen of ApoE$^{-/-}$ mice (Fig. 3I, J). These data indicate that ^{18}F-FLT reflects increased hematopoietic activity in the marrow and spleen of mice with atherosclerosis, in accordance with the previous description of increased bone marrow hematopoiesis in atherosclerotic mice[12] and the reactivation of extramedullary, i.e. splenic hematopoiesis in atherosclerosis[13].

Hematopoietic activation with a Toll like receptor ligand increases ^{18}F-FLT signal

Hematopoiesis provides billions of blood cells every day, and increases the production of leukocytes according to numerous stimuli. For instance, HSPCs express TLR4 on their surface, and TLR4 ligation increases proliferation, differentiation and output of mature cells, including monocytes[14]. We therefore hypothesized that the changes observed in hematopoietic organs of mice with atherosclerosis could be reproduced with LPS, a bacterial TLR4 ligand that strongly stimulates hematopoiesis[14]. Wild-type mice that received LPS showed increased bone marrow uptake of ^{18}F-FLT (Fig. 4A, B) that paralleled results of ex vivo scintillation counting (Fig. 4C). In accordance with the observed uptake of ^{18}F-FLT, a higher fraction of LSK was in the active cell cycle phase after LPS injection (Fig. 4D, E). TLR4 ligands induce HSPC migration from the bone marrow to the spleen, where the cells seed extramedullary niches. Indeed, splenic uptake of ^{18}F-FLT was increased, as observed by in vivo imaging (Fig. 4F, G) and ex vivo scintillation counting (Fig. 4H). In parallel, the

number of cycling LSK increased dramatically in spleens of mice that received LPS (Fig. 4I, J).

Dampening of hematopoiesis with 5-FU decreases ^{18}F-FLT signal

Next we explored whether ^{18}F-FLT signal might also monitor a decrease of hematopoietic activity. To test this hypothesis, we treated wild-type mice with 5-FU, a clinical drug that is frequently employed in hematology research to ablate cycling stem cells. Previously, 5-FU reduced ^{18}F-FLT signal in tumor bearing mice[15]. Treatment with 5-FU reduced bone marrow uptake of ^{18}F-FLT measured in vivo (Fig. 5A, B) and ex vivo (Fig. 5C). As expected, 5-FU decreased proliferation of bone marrow LSK (Fig. 5D, E). The spleen showed a similar pattern: 5-FU treatment reduced ^{18}F-FLT signal (Fig. 5G,H) and the frequency of proliferating LSK in parallel (Fig. 5I, J).

In vitro ^{18}F-FLT uptake

To better understand cellular ^{18}F-FLT uptake, we pursued in vitro incubation of the tracer in primary murine cells. Peritoneal macrophages were isolated by negative magnetic bead selection and either treated with 5-FU or not. Scintillation counting revealed that macrophages that were not treated with 5-FU showed higher uptake of the PET tracer (Fig. 6A). FACS analysis of these samples reported decreased staining for the proliferation marker Ki67 (Fig. 6B, C). Further, we used positive magnetic bead selection of murine bone marrow to enrich for c-kit$^+$ progenitor cells and Ly6G$^+$ neutrophils. Incubation of these cells with ^{18}F-FLT was followed by scintillation counting. We detected higher uptake of ^{18}F-FLT into c-kit$^+$ cells (Fig. 6D), and flow cytometry documented their higher proliferative activity when compared to Ly-G$^+$ cells (Fig. 6E,F). Of note, these data do not confer specificity of the PET tracer to progenitor cells but rather indicate that proliferating cells, including c-kit$^+$ progenitor cells, have a higher propensity to take up the imaging agent.

^{18}F-FLT PET in rabbits with atherosclerosis

To study ^{18}F-FLT plaque uptake in a different species, we subjected 4 rabbits with atherosclerosis and balloon injury and 4 control rabbits without atherosclerosis to PET/CT imaging. MRI confirmed that the treatment induced robust atherosclerotic lesions in the infrarenal aorta (Fig. 7A). Rabbits first underwent ^{18}F-FDG PET imaging, which showed a heterogeneous pattern of inflammatory activity (Fig. 7B). As expected, the ^{18}F-FDG signal was significantly higher in the aortic segments of rabbits with atherosclerosis (SUV mean controls, 0.20 ± 0.002; atherosclerosis cohort, 0.58 ± 0.02, $p<0.0001$). Immunohistochemistry of anti-rabbit macrophage (RAM11) staining demonstrated abundant macrophages in the atherosclerosis of these rabbits (Fig. 7C). Previous correlation of ^{18}F-FDG to histology in atherosclerotic rabbits[16] and in humans[17] showed that ^{18}F-FDG PET signal increases with higher macrophage plaque burden. Within 48 hours of the ^{18}F-FDG PET, rabbits were rescanned after injection of ^{18}F-FLT, enabling a comparison of both PET agents. Pharmacokinetic experiments revealed a blood half-life of 20.36 ± 3.54 minutes for ^{18}F-FLT in atherosclerotic rabbits and an optimal injection-imaging sequence of 200 minutes. The aortic ^{18}F-FLT signal was higher in rabbits with atherosclerosis when compared to control rabbits without atherosclerosis (Fig. 7D, E). We used the ^{18}F-FDG data to classify 3 aortic regions in rabbits with atherosclerosis: low (SUV<0.4), intermediate

(0.4–0.6) and high grade inflammation (SUV>0.6). The vascular territories that were classified as high-grade inflammation showed the highest ^{18}F-FLT signal (Fig. 7F, G). Linear regression analysis in aortic segments of rabbits with atherosclerosis revealed that ^{18}F-FLT and ^{18}F-FDG signal were weakly positively correlated (Fig. 7H), whereas no correlation was detected in control rabbits.

^{18}F-FLT PET in humans with atherosclerosis

To assess the potential of ^{18}F-FLT for PET imaging of proliferation in human atherosclerotic plaque, we performed a retrospective analysis of ten patients with high risk of cardiovascular disease (atherosclerosis group) and ten patients with a low cardiovascular risk profile (control group) that were originally imaged because of malignant disease and stratified by Framingham Scoring (Table 1). We found that patients with high cardiovascular risk showed intense calcification, indicative of atherosclerotic lesions (Fig. 8A). Patients had undergone both, ^{18}F-FDG and ^{18}F-FLT PET imaging (Fig. 8B, C). Analysis of the ascending aorta (Fig. 8D–G) and the carotid artery (Fig. 8H–K) showed increased vascular uptake of both PET agents in the individuals with high cardiovascular risk. As observed in rabbits, linear regression analysis in aortic segments showed a weak positive correlation between ^{18}F-FLT and ^{18}F-FDG uptake (Fig. 8L).

DISCUSSION

Why are we interested in imaging macrophage proliferation? In inflamed tissue, these cells have a short to intermediate life span, ranging from hours to weeks. In mice with atherosclerosis, the entire plaque macrophage population turns over in one month[3]. Provision of mononuclear phagocytes influences atherosclerosis progression and plaque characteristics[2]. Depleting macrophages and monocytes or inhibiting their recruitment to plaque reproducibly diminishes atherosclerosis in animals. While a number of interventions may influence macrophage proliferation, non-invasive imaging reporting on this process could markedly facilitate drug development by informing dose selection, and providing an early biomarker of effective targeting. Oncology and neurodegenerative research adopted such companion-imaging strategies for rapid, non-invasive feed-back on the targeted pathway or molecule in small numbers of patients. Such information would inform study design and the triage of candidates to advance into large scale trials, enabling a nimbler drug development strategy[18].

Tissue-resident macrophages proliferate everywhere[19]. All major organ systems, including the vasculature, heart and brain host a network of non-inflammatory stromal macrophages. These cells have as of yet unclear functions, but they may promote tissue homeostasis, defense and regeneration[20]. We found that most healthy organs had low ^{18}F-FLT baseline uptake, likely reflecting the low proliferative rate of stromal cells and tissue macrophages. The bone marrow, intestine, kidney and liver furnish notable exceptions, as reported previously[5]. These organs have high baseline proliferative activity, or participate in the excretion of ^{18}F-FLT.

HSPCs increase proliferative activity in the bone marrow in atherosclerosis, after myocardial infarction and after stroke[12, 21, 22]. Circulating danger signals may also directly

alert HSPCs to remote organ ischemic or other injury[2]. Compromised reverse cholesterol transport induces increased HSPC activity, linking metabolism to monocyte production[12]. Monocyte numbers in blood then rise with progressing hyperlipidemia[23] and associate with poor prognosis[2]. Cardiovascular disease also reactivates splenic leukocyte production. Gradually in mice with atherosclerosis[13], and rapidly after ischemia[22], HSPCs seed the splenic red pulp and expand monocyte production. Splenic HSPC retention relies on VCAM-1 expression by $CD169^+$ macrophages[24]. GM-CSF, M-CSF and IL-3 mediate splenic myelopoiesis[13, 24]. Indeed, increased splenic and bone marrow ^{18}F-FDG uptake associates with higher cardiovascular event rates in patients[25]. The decisive contribution of local proliferation to the enlarged macrophage pool in atherosclerotic lesions engendered interest in this process[3]. In mice with mature lesions, genetic deficiency of scavenger receptor A reduces incorporation of the thymidine analog BrdU into lesional macrophages[3]. These pathways may have contributed to the increased ^{18}F-FLT PET signal observed in the present study, and their exploration as therapeutic targets will benefit from an imaging biomarker such as ^{18}F-FLT PET.

Rabbits with atherosclerosis displayed increased ^{18}F-FLT signal in vascular territories with high ^{18}F-FDG uptake. However, the correlation between both tracers in aortic segments of atherosclerotic rabbits and patients was weak. ^{18}F-FDG is trapped inside cells with high glucose uptake and correlates with macrophage number in the atherosclerotic plaque in rabbits and humans[16, 17]. Macrophage accumulation depends on increased proliferation and on monocyte recruitment. The observation of matching tracer uptake in some aortic segments supports that ^{18}F-FLT enriches in plaques with high macrophage proliferation, as cell growth and proliferation are energy-intensive processes. In distinction to ^{18}F-FLT, ^{18}F-FDG is not specific for proliferating cells. Thus, some aortic segments high in ^{18}F-FDG may have a high glucose uptake but low proliferating rates. Taken together, ^{18}F-FLT may be a useful to study macrophage supply while reducing proliferation of hematopoietic cells. Myocardial uptake of ^{18}F-FDG can interfere with coronary artery imaging, a limitation that does not occur with ^{18}F-FLT.

As indicated by its use for imaging proliferating cancer cells, ^{18}F-FLT is not specific for macrophages or hematopoietic progenitor cells. Parenchymal cells that proliferate in plaque or hematopoietic organs may contribute to the observed signal, including endothelial and smooth muscle cells. This is a significant limitation of ^{18}F-FLT PET imaging, which is perhaps counterbalanced by its clinical availability. Our histological data imply, however, that most $Ki67^+$ plaque cells were macrophages. A strategy to increase specificity for macrophages could rely on multimodal PET/MRI, in which ^{18}F-FLT PET could be combined with iron oxide macrophage MRI. ^{18}F-FLT signal colocalization with T2* MR signal decrease may confer increased cellular specificity. ^{18}F-FLT has not shown adverse effects in clinical imaging trials, paving the way for a prospective trial that correlates ^{18}F-FLT signal in plaque and hematopoietic organs with clinical outcome.

Supplementary Material

Refer to Web version on PubMed Central for supplementary material.

Acknowledgments

SOURCES OF FUNDING: This work was funded by grants from the National Institute of Health HL114477, HL117829, HL096576, HL118440, HL125703, HL071021, EB009638, the Deutsche Herzstiftung (S/05/12) and the MGH Research Scholar Award.

Nonstandard abbreviations and Acronyms

5-FU	fluorouracil
ApoE$^{-/-}$	apolipoprotein E knock out
BrdU	Bromodeoxyuridine
^{18}F-FDG	^{18}F-fluorodeoxyglucose
^{18}F-FLT	3'-Deoxy-3'-[^{18}F]-fluorothymidine
HPLC	high-performance liquid chromatography
HSPCs	hematopoietic stem and progenitor cells
LPS	lipopolysaccharide
LSK	lineage^{-} Sca-1^{+} C-kit^{+} progenitor cells
PET	positron emission tomography
ROI	region of interest
SUV	standardized uptake value
TLR	Toll-like receptor

References

1. Libby P. Inflammation in atherosclerosis. Nature. 2002; 420:868–874. [PubMed: 12490960]
2. Swirski FK, Nahrendorf M. Leukocyte behavior in atherosclerosis, myocardial infarction, and heart failure. Science. 2013; 339:161–166. [PubMed: 23307733]
3. Robbins CS, Hilgendorf I, Weber GF, Theurl I, Iwamoto Y, Figueiredo JL, Gorbatov R, Sukhova GK, Gerhardt LM, Smyth D, Zavitz CC, Shikatani EA, Parsons M, van Rooijen N, Lin HY, Husain M, Libby P, Nahrendorf M, Weissleder R, Swirski FK. Local proliferation dominates lesional macrophage accumulation in atherosclerosis. Nat Med. 2013; 19:1166–1172. [PubMed: 23933982]
4. Shields AF, Grierson JR, Dohmen BM, Machulla HJ, Stayanoff JC, Lawhorn-Crews JM, Obradovich JE, Muzik O, Mangner TJ. Imaging proliferation in vivo with [F-18]FLT and positron emission tomography. Nat Med. 1998; 4:1334–1336. [PubMed: 9809561]
5. Bading JR, Shields AF. Imaging of cell proliferation: status and prospects. J Nucl Med. 2008; 49(Suppl 2):64S–80S. [PubMed: 18523066]
6. Chalkidou A, Landau DB, Odell EW, Cornelius VR, O'Doherty MJ, Marsden PK. Correlation between Ki-67 immunohistochemistry and 18F-fluorothymidine uptake in patients with cancer: A systematic review and meta-analysis. Eur J Cancer. 2012; 48:3499–3513. [PubMed: 22658807]
7. Zhang CC, Yan Z, Li W, Kuszpit K, Painter CL, Zhang Q, Lappin PB, Nichols T, Lira ME, Affolter T, Fahey NR, Cullinane C, Spilker M, Zasadny K, O'Brien P, Buckman D, Wong A, Christensen JG. [(18)F]FLT-PET imaging does not always "light up" proliferating tumor cells. Clin Cancer Res. 2012; 18:1303–1312. [PubMed: 22170262]
8. McKinley ET, Ayers GD, Smith RA, Saleh SA, Zhao P, Washington MK, Coffey RJ, Manning HC. Limits of [18F]-FLT PET as a biomarker of proliferation in oncology. PLoS One. 2013; 8:e58938. [PubMed: 23554961]

9. Agool A, Schot BW, Jager PL, Vellenga E. 18F-FLT PET in hematologic disorders: a novel technique to analyze the bone marrow compartment. J Nucl Med. 2006; 47:1592–1598. [PubMed: 17015893]
10. McGuire SM, Menda Y, Boles Ponto LL, Gross B, TenNapel M, Smith BJ, Bayouth JE. Spatial mapping of functional pelvic bone marrow using FLT PET. J Appl Clin Med Phys. 2014; 15:4780. [PubMed: 25207403]
11. Calcagno C, Cornily JC, Hyafil F, Rudd JH, Briley-Saebo KC, Mani V, Goldschlager G, Machac J, Fuster V, Fayad ZA. Detection of neovessels in atherosclerotic plaques of rabbits using dynamic contrast enhanced MRI and 18F-FDG PET. Arterioscler Thromb Vasc Biol. 2008; 28:1311–1317. [PubMed: 18467641]
12. Yvan-Charvet L, Pagler T, Gautier EL, Avagyan S, Siry RL, Han S, Welch CL, Wang N, Randolph GJ, Snoeck HW, Tall AR. ATP-binding cassette transporters and HDL suppress hematopoietic stem cell proliferation. Science. 2010; 328:1689–1693. [PubMed: 20488992]
13. Robbins CS, Chudnovskiy A, Rauch PJ, Figueiredo JL, Iwamoto Y, Gorbatov R, Etzrodt M, Weber GF, Ueno T, van Rooijen N, Mulligan-Kehoe MJ, Libby P, Nahrendorf M, Pittet MJ, Weissleder R, Swirski FK. Extramedullary hematopoiesis generates Ly-6C(high) monocytes that infiltrate atherosclerotic lesions. Circulation. 2012; 125:364–374. [PubMed: 22144566]
14. Nagai Y, Garrett KP, Ohta S, Bahrun U, Kouro T, Akira S, Takatsu K, Kincade PW. Toll-like receptors on hematopoietic progenitor cells stimulate innate immune system replenishment. Immunity. 2006; 24:801–812. [PubMed: 16782035]
15. Barthel H, Cleij MC, Collingridge DR, Hutchinson OC, Osman S, He Q, Luthra SK, Brady F, Price PM, Aboagye EO. 3′-deoxy-3′-[18F]fluorothymidine as a new marker for monitoring tumor response to antiproliferative therapy in vivo with positron emission tomography. Cancer Res. 2003; 63:3791–3798. [PubMed: 12839975]
16. Tawakol A, Migrino RQ, Hoffmann U, Abbara S, Houser S, Gewirtz H, Muller JE, Brady TJ, Fischman AJ. Noninvasive in vivo measurement of vascular inflammation with F-18 fluorodeoxyglucose positron emission tomography. J Nucl Cardiol. 2005; 12:294–301. [PubMed: 15944534]
17. Tawakol A, Migrino RQ, Bashian GG, Bedri S, Vermylen D, Cury RC, Yates D, LaMuraglia GM, Furie K, Houser S, Gewirtz H, Muller JE, Brady TJ, Fischman AJ. In vivo 18F-fluorodeoxyglucose positron emission tomography imaging provides a noninvasive measure of carotid plaque inflammation in patients. J Am Coll Cardiol. 2006; 48:1818–1824. [PubMed: 17084256]
18. Mulder WJ, Jaffer FA, Fayad ZA, Nahrendorf M. Imaging and nanomedicine in inflammatory atherosclerosis. Sci Transl Med. 2014; 6:239sr1. [PubMed: 24898749]
19. Davies LC, Jenkins SJ, Allen JE, Taylor PR. Tissue-resident macrophages. Nat Immunol. 2013; 14:986–995. [PubMed: 24048120]
20. Nahrendorf M, Swirski FK. Monocyte and macrophage heterogeneity in the heart. Circ Res. 2013; 112:1624–1633. [PubMed: 23743228]
21. Courties G, Herisson F, Sager HB, Heidt T, Ye Y, Wei Y, Sun Y, Severe N, Dutta P, Scharff J, Scadden DT, Weissleder R, Swirski FK, Moskowitz MA, Nahrendorf M. Ischemic stroke activates hematopoietic bone marrow stem cells. Circ Res. 2015; 116:407–417. [PubMed: 25362208]
22. Dutta P, Courties G, Wei Y, Leuschner F, Gorbatov R, Robbins CS, Iwamoto Y, Thompson B, Carlson AL, Heidt T, Majmudar MD, Lasitschka F, Etzrodt M, Waterman P, Waring MT, Chicoine AT, van der Laan AM, Niessen HW, Piek JJ, Rubin BB, Butany J, Stone JR, Katus HA, Murphy SA, Morrow DA, Sabatine MS, Vinegoni C, Moskowitz MA, Pittet MJ, Libby P, Lin CP, Swirski FK, Weissleder R, Nahrendorf M. Myocardial infarction accelerates atherosclerosis. Nature. 2012; 487:325–329. [PubMed: 22763456]
23. Swirski FK, Libby P, Aikawa E, Alcaide P, Luscinskas FW, Weissleder R, Pittet MJ. Ly-6Chi monocytes dominate hypercholesterolemia-associated monocytosis and give rise to macrophages in atheromata. J Clin Invest. 2007; 117:195–205. [PubMed: 17200719]
24. Dutta P, Hoyer FF, Grigoryeva LS, Sager HB, Leuschner F, Courties G, Borodovsky A, Novobrantseva T, Ruda VM, Fitzgerald K, Iwamoto Y, Wojtkiewicz G, Sun Y, Da Silva N, Libby P, Anderson DG, Swirski FK, Weissleder R, Nahrendorf M. Macrophages retain hematopoietic stem cells in the spleen via VCAM-1. J Exp Med. 2015; 212:497–512. [PubMed: 25800955]

25. Emami H, Singh P, MacNabb M, Vucic E, Lavender Z, Rudd JH, Fayad ZA, Lehrer-Graiwer J, Korsgren M, Figueroa AL, Fredrickson J, Rubin B, Hoffmann U, Truong QA, Min JK, Baruch A, Nasir K, Nahrendorf M, Tawakol A. Splenic metabolic activity predicts risk of future cardiovascular events: demonstration of a cardiosplenic axis in humans. JACC Cardiovasc Imaging. 2015; 8:121–130. [PubMed: 25577441]

Novelty and Significance

What Is Known?

- Macrophages promote disease progression in atherosclerosis.
- The turnover of macrophages is rapid, making it interesting to study their supply.
- Macrophages derive either from monocytes, which are progeny of hematopoietic stem cells in the marrow and spleen, or, especially in mature plaque, from local proliferation.

What New Information Does This Article Contribute?

- ^{18}F-FLT, a thymidine analog that avidly incorporates into proliferating cells, enriches in atherosclerotic plaque of mice, rabbits and human patients.
- While other stromal cells contribute, the majority of proliferating cells in atherosclerotic lesions are macrophages.
- ^{18}F-FLT PET-CT imaging reports increased activity in the hematopoietic organs of mice with atherosclerosis.
- ^{18}F-FLT plaque uptake increases with the duration of diet exposure in ApoE$^{-/-}$ mice.
- Originally developed for imaging proliferation in malignant disease, this PET imaging method may allow monitoring the expansion of hematopoietic cells in the setting of atherogenesis.

Myeloid cells are key protagonists in the progression of atherosclerotic disease. In inflammation, their life span is considerably shortened, which motivated the field's recently emerging interest in the production of these cells. The small molecule PET tracer ^{18}F-FLT is an analog to the DNA building block thymidine. Just like BrdU, another thymidine analog used to measure cell proliferation, it incorporates into cells that are actively cycling. Our data suggest that ^{18}F-FLT PET-CT imaging may be a clinically available method to study hematopoietic activity in patients with atherosclerosis. This could be of particular value in testing novel anti-atherosclerotic therapies designed to diminish macrophage infiltration into inflammatory atherosclerotic plaques.

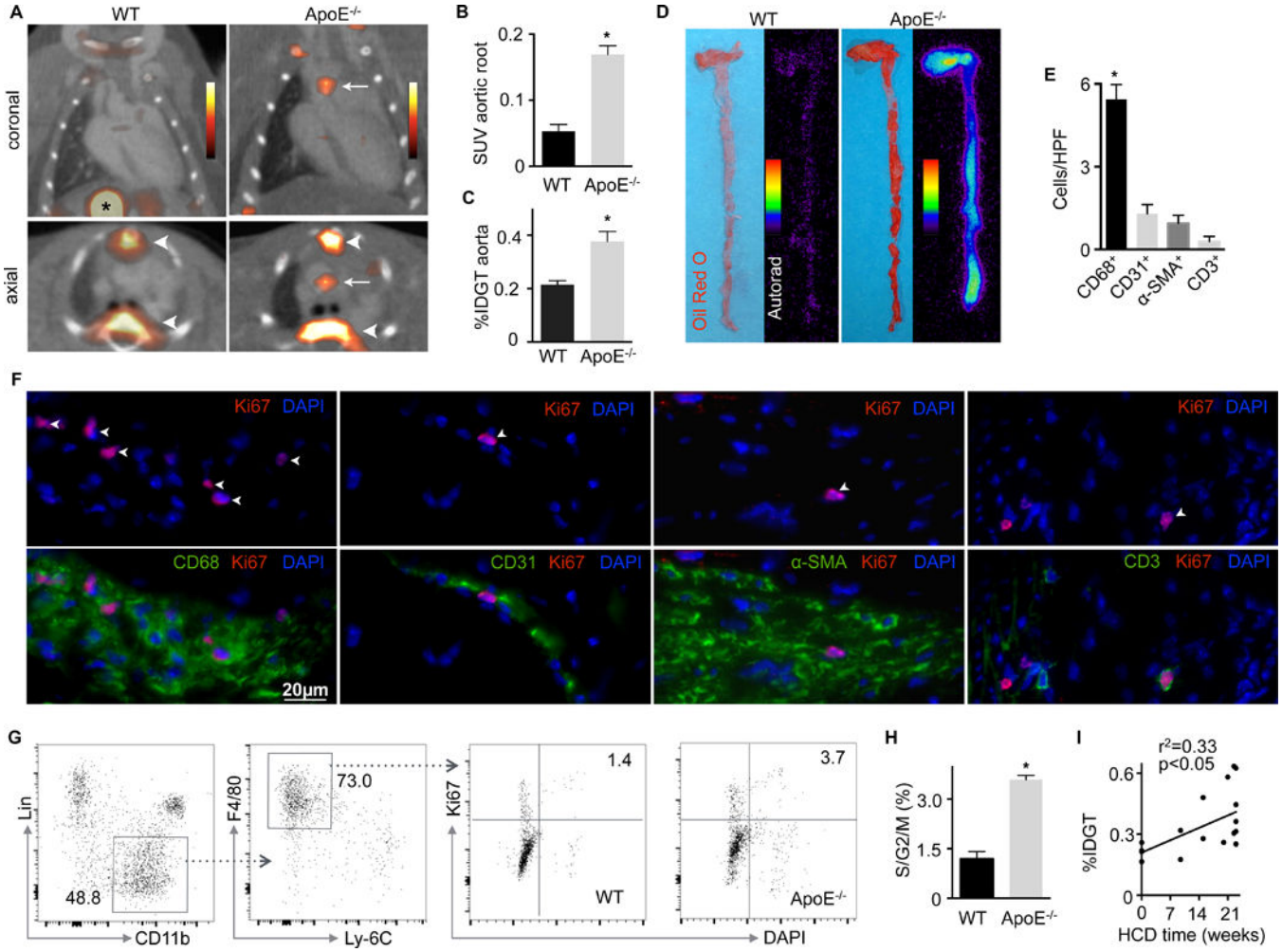

Figure 1. ^{18}F-FLT uptake in mice with atherosclerosis

(A) PET-CT images show higher ^{18}F-FLT uptake in atherosclerotic lesions (arrow) of ascending aorta in an ApoE$^{-/-}$ compared to a wild-type mouse. High ^{18}F-FLT signal also appears in the sternum and vertebrae (arrow heads) and gallbladder (asterisk). (B and C) Bar graphs show in vivo SUV (WT, n=5; ApoE$^{-/-}$, n=13) and ex vivo %IDGT in the aorta (WT, n=5; ApoE$^{-/-}$, n=15). (D) Oil red O staining of aortae illustrates co-localization of ^{18}F-FLT signal with atherosclerotic lesions. (E) Quantification of proliferating macrophages (CD68^{+}), endothelial cells (CD31^{+}), smooth muscle cells (α-SMA^{+}) and T cells (CD3^{+}) per high power field (HPF). (F) Example stains with anti Ki-67 and anti CD68 mAbs show proliferating macrophages (arrow heads), smooth muscle cells (α-SMA^{+}) and T cells (CD3^{+}) in the atherosclerotic lesion. (G) Flow cytometry plots and (H) quantitative data reveal increased proliferation of macrophages in atherosclerotic aortae (WT, n=8; ApoE$^{-/-}$, n=10). (I) Correlation between aortic %IDGT and the duration of high cholesterol diet (HCD) measured in wild type (HCD = 0) and ApoE$^{-/-}$ aortae (HCD > 0). Data are mean ±SEM. *P<0.05, Student's t-test.

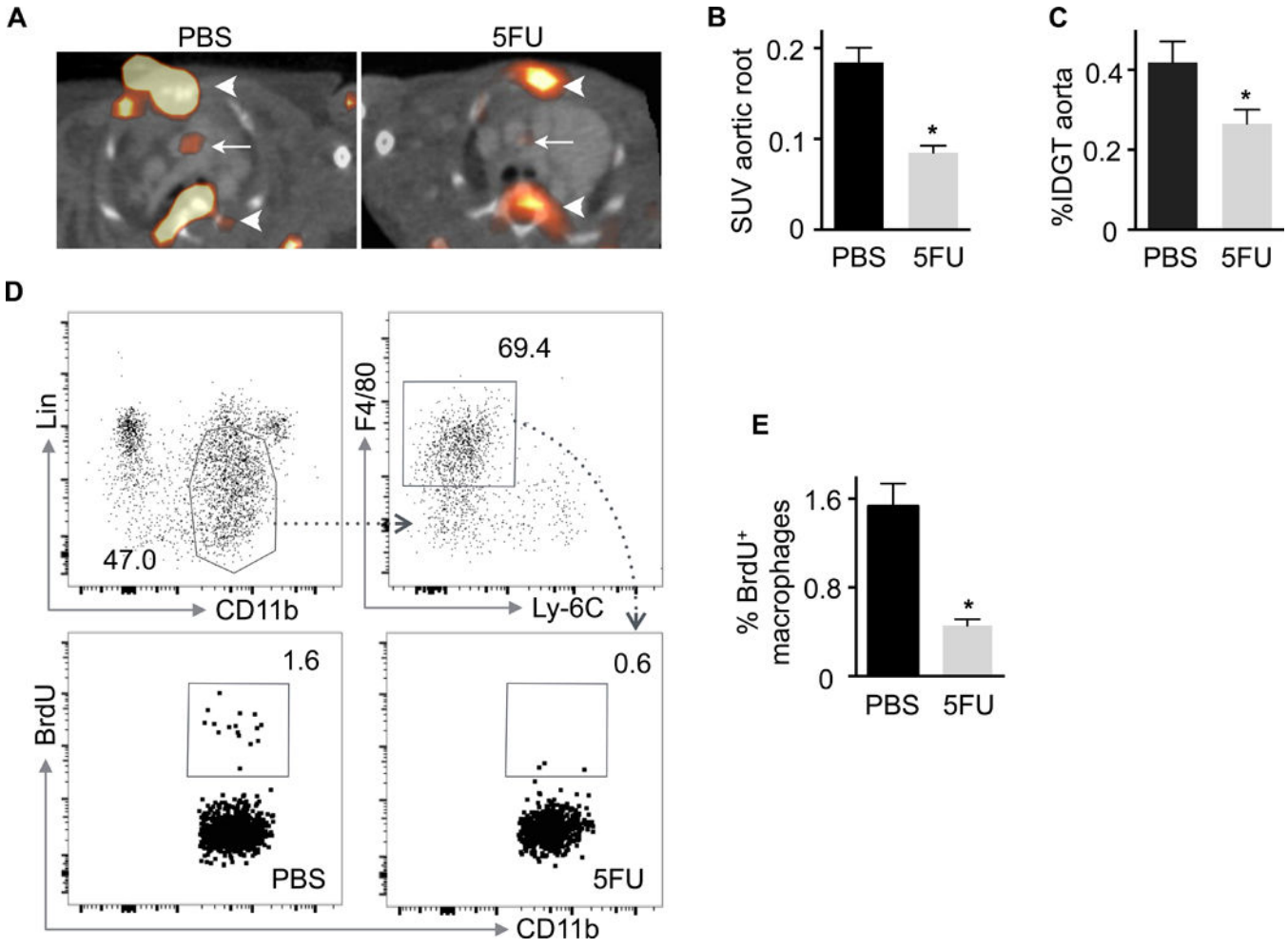

Figure 2. 5-FU treatment reduced ^{18}F-FLT uptake in murine atherosclerotic plaque

(A) PET-CT images show reduced ^{18}F-FLT uptake in atherosclerotic lesions (arrow) of ascending aorta in an ApoE$^{-/-}$ mouse after 5-FU injection, compared to the control ApoE$^{-/-}$ mouse with PBS injection. Arrow heads indicate sternum and vertebrae. (B and C) Bar graphs show in vivo SUV (PBS, n=9; 5-FU, n=5) and ex vivo %IDGT in the aorta (PBS, n=10; 5-FU, n=6). (D) Flow cytometry plots and (E) quantitative data show significantly lower proliferation of macrophages in aortae after 5-FU treatment (PBS, n=4; 5-FU, n=6). Data are mean±SEM. *P<0.05, Student's t-test.

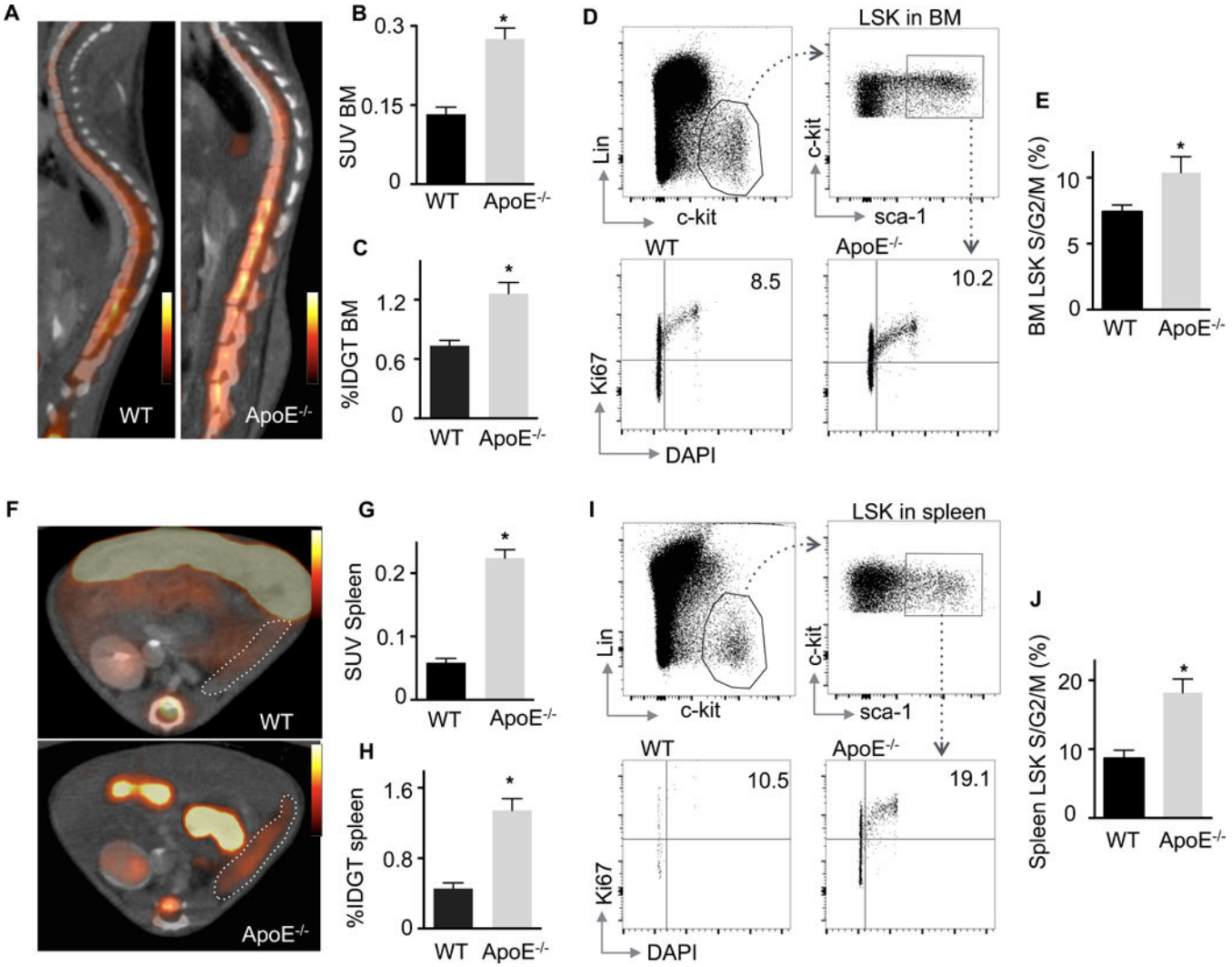

Figure 3. Increased uptake of ^{18}F-FLT in bone marrow and spleen of ApoE$^{-/-}$ mice

(A) In vivo PET-CT shows higher uptake of ^{18}F-FLT in the spine of an ApoE$^{-/-}$ when compared to a wild-type mouse (WT). (B) In vivo SUV (WT, n=5; ApoE$^{-/-}$, n=13) and (C) ex vivo %IDGT (WT, n=5; ApoE$^{-/-}$, n=15) in bone marrow. (D) Flow cytometry plots and (E) quantitative cell cycle analysis of LSK cells in bone marrow of ApoE$^{-/-}$ and wild-type mice (WT, n=12; ApoE$^{-/-}$, n=10). (F) Representative in vivo PET-CT images of spleen. (G) In vivo SUV (WT, n=5; ApoE$^{-/-}$, n=13) and (H) ex vivo scintillation counting of spleens from ApoE$^{-/-}$ and wild-type mice (WT, n=5; ApoE$^{-/-}$, n=15). (I) Flow cytometry plots and (J) quantitative cell cycle analysis of LSK cells in spleens of ApoE$^{-/-}$ and wild-type mice (WT, n=8; ApoE$^{-/-}$, n=10). Data are presented as mean±SEM. *P<0.05, Student's t-test.

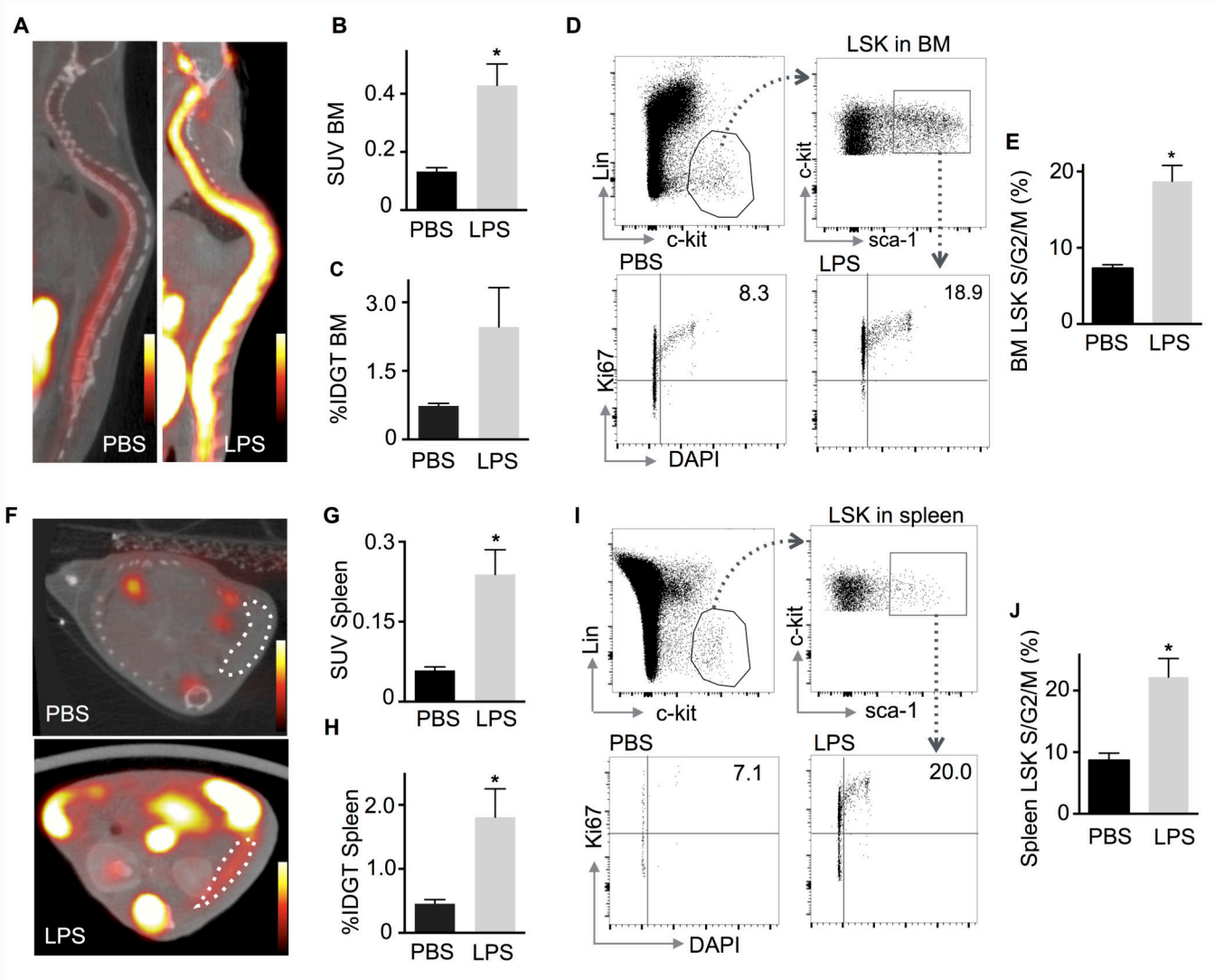

Figure 4. ^{18}F-FLT uptake in bone marrow and the spleen after LPS challenge

(A) In vivo PET-CT visualizes elevated ^{18}F-FLT signal in the spine of wild-type mice after LPS challenge in comparison to mice after a control saline injection (PBS). (B) In vivo SUV (PBS, n=5; LPS, n=6) and (C) ex vivo %IDGT were increased in bone marrow after LPS (PBS, n=5; LPS, n=6, p=0.052). (D, E) Flow cytometry analysis of bone marrow revealed significantly increased proliferation of hematopoietic progenitor cells (LSK) after LPS (PBS, n=13; LPS, n=6). (F) In vivo PET-CT of the spleen in wild-type mice after LPS challenge in comparison to mice after PBS injection. (G) In vivo SUV (PBS, n=5; LPS, n=6) and (H) ex vivo %IDGT in spleen after LPS challenge (PBS, n=5; LPS, n=6). (I) Flow cytometry plots and (J) bar graph shows cell cycle analysis of LSK in the spleen (PBS, n=8; LPS, n=6). Data are shown as mean±SEM. *P<0.05, Student's t-test.

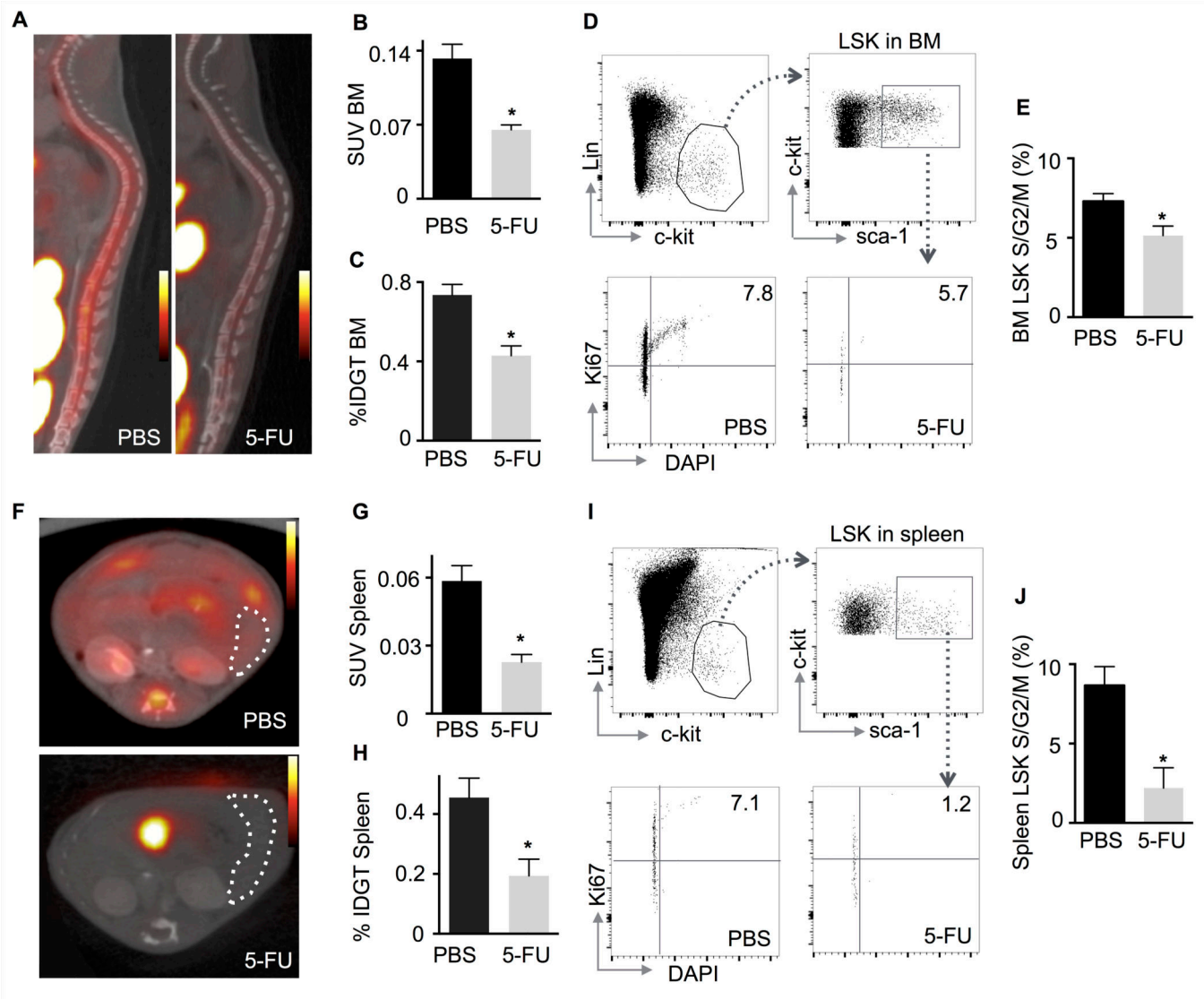

Figure 5. Decrease of ^{18}F-FLT update in hematopoietic organs after 5-FU treatment

(A) In vivo PET-CT shows reduced ^{18}F-FLT signal in the spine of wild-type mice after 5-FU injection, in comparison to animals with control saline injection (PBS). (B) In vivo SUV (PBS, n=5; 5-FU, n=5) and (C) ex vivo scintillation counting (%IDGT, PBS, n=5; 5-FU, n=7) were measured in bone marrow. (D, E) Flow cytometry analysis of bone marrow LSK cells in 5-FU treated mice (PBS, n=13; 5-FU, n=7). (F) In vivo PET-CT images of the spleen after 5-FU application. (G) In vivo SUV (PBS, n=5; 5-FU, n=5) and (H) ex vivo scintillation counting (%IDGT, PBS, n=5; 5-FU, n=7) of the spleen. (I) Flow cytometric plots and (J) quantitative cell cycle analysis of spleen LSK (PBS, n=8; 5-FU, n=7). Data are mean±SEM. *P<0.05, Student's t-test.

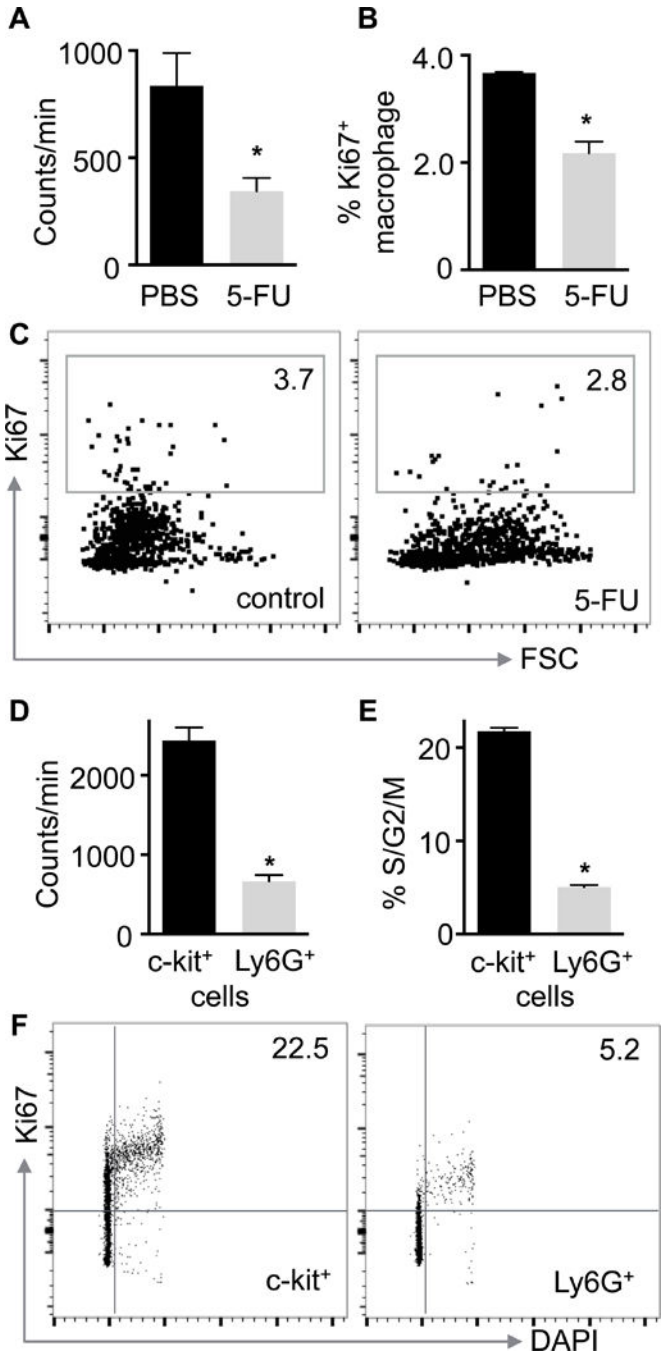

Figure 6. ^{18}F-FLT uptake into myeloid and progenitor cells

(A) Gamma counting of 5-FU treated and non-treated control peritoneal macrophages after ^{18}F-FLT incubation for 60 minutes. (B) Bar graph and (C) dot plots of flow cytometry show frequency of Ki67$^+$ macrophages by flow cytometry. (D) Gamma counting of bone marrow c-kit$^+$ and Ly6G$^+$ cells after ^{18}F-FLT incubation for 60 minutes. (E) Bar graph and (F) dot plots of flow cytometry showing frequency of cells in S/G2/M phase for Ly6G$^+$ versus c-kit$^+$ cells. Experiments were done in triplicates. Data are mean±SEM. *P<0.05, Student's t-test.

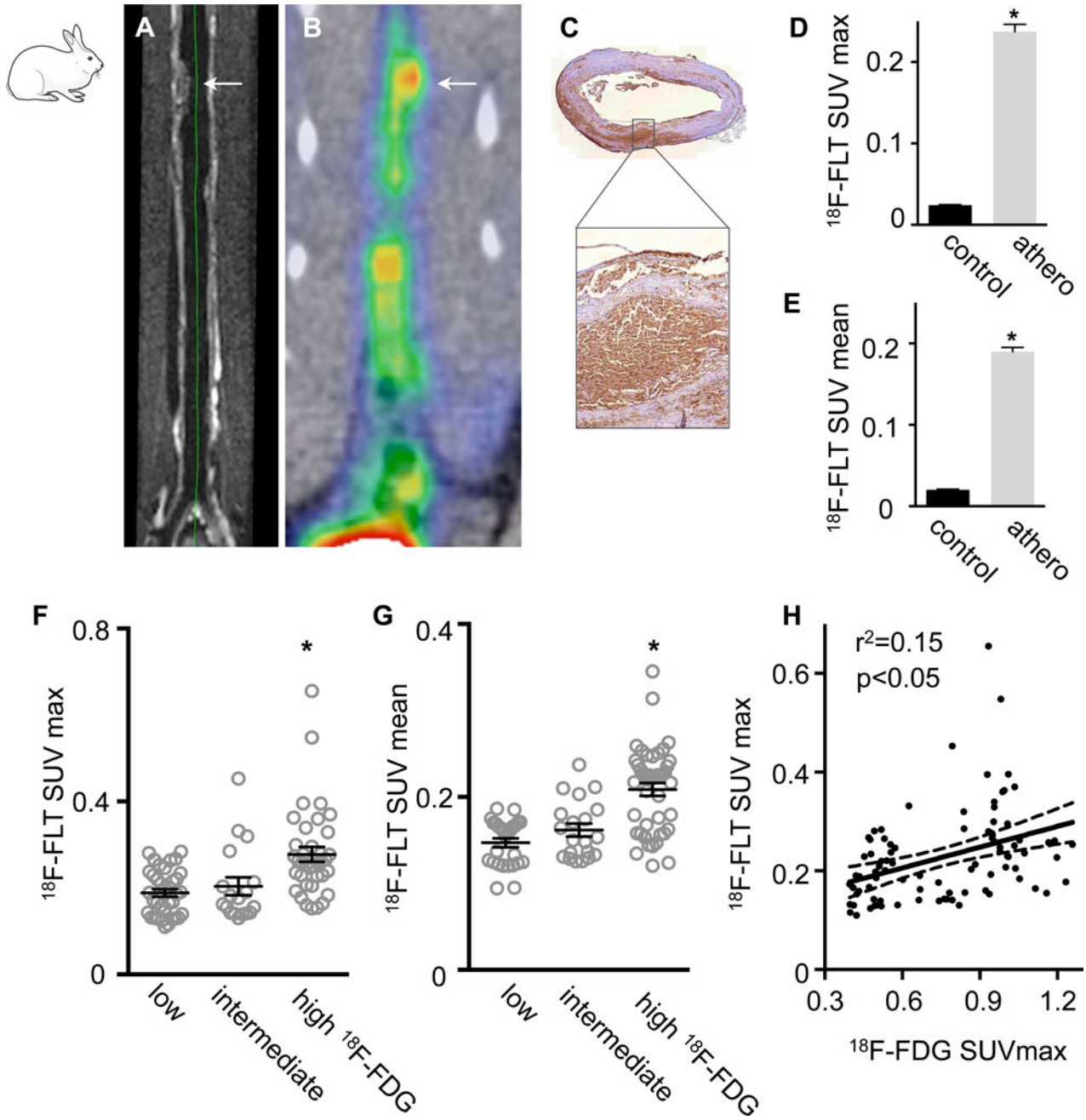

Figure 7. ^{18}F-FLT and ^{18}F-FDG PET-CT in rabbits with atherosclerosis

(A) MRI confirms presence of atherosclerotic lesions in the descending rabbit aorta (arrow). (B) Heterogeneous inflammatory patterns are indicated by ^{18}F-FDG PET-CT of the same region. (C) Immunohistochemistry of anti-rabbit macrophage (RAM-11) staining shows abundant macrophages in the atherosclerotic lesions. (D) ^{18}F-FLT SUV max and (E) ^{18}F-FLT SUV mean in aortae of rabbit cohorts with and without atherosclerosis (n=4 per group). (F, G) Aortic regions that were grouped for low (SUV mean <0.4), intermediate (0.4–0.6) and high ^{18}F-FDG signal (>0.6) in a total of 4 rabbits with atherosclerosis. Data are mean

±SEM. *P<0.05, Mann-Whitney test. (H) Linear regression of ^{18}F-FDG and ^{18}F-FLT SUV max in aortic segments of 4 rabbits with atherosclerosis.

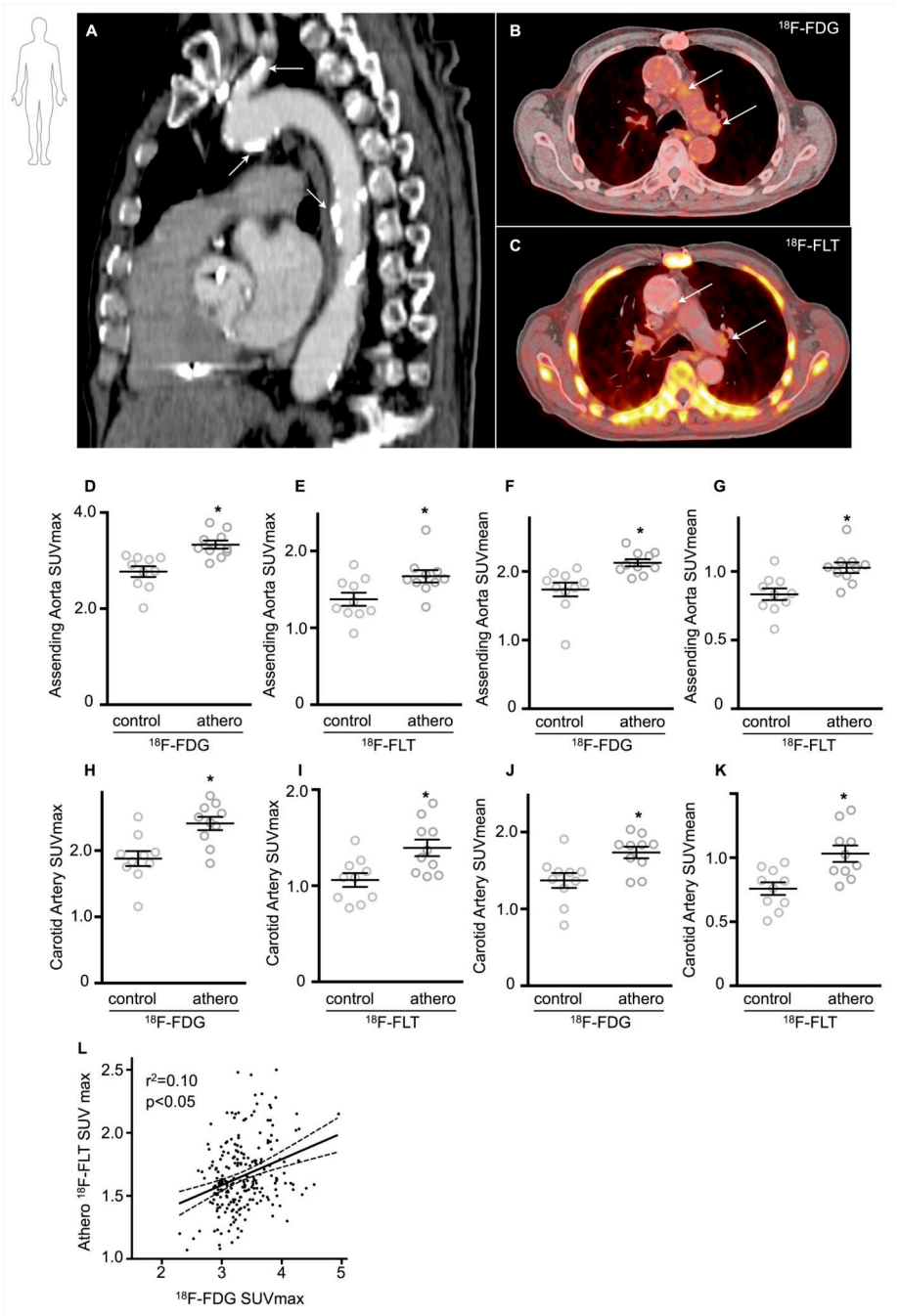

Figure 8. ^{18}F-FLT and ^{18}F-FDG PET-CT in humans with atherosclerosis

(A) Sagittal image revealing extensive calcification in the aorta and carotid artery (arrows). ^{18}F-FDG (B) and ^{18}F-FLT (C) images demonstrate uptake of the PET tracers in the vessel wall of the aortic arch (arrows). (D-G) In the ascending aorta, ^{18}F-FDG and ^{18}F-FLT uptake was significantly higher in the atherosclerotic patients when compared to low-risk subjects. (H-K) In the common carotid artery both ^{18}F-FDG and ^{18}F-FLT uptake was

significantly higher in atherosclerotic patients. *P<0.05, Student's t-test. (L) Linear regression of ^{18}F-FDG and ^{18}F-FLT SUV max in aortic segments.

Table 1

Patient demographics

	Atherosclerosis	Controls	p-value
Risk assessment, 10 year risk Framingham score, %	20 (15–30)	2 (1–4)	<0.001
Gender (n)			
male	8 (80%)	8 (80%)	
Age (years)			
Mean (range)	73 (65 – 87)	51 (40 – 63)	<0.001
Smoking			
Yes	2(20%)	1 (10%)	
Systolic blood pressure, mmHg			
Mean (range)	163 (130 – 191)	127 (103 – 160)	<0.001
Anti-hypertensive treatment			
Yes	9 (90%)	0 (0%)	<0.001
Time between ^{18}F-FDG and ^{18}F-FLT scan (days)			
Mean (range)	4 (1 – 13)	4 (2–7)	
Injected dose (MBq)			
^{18}F-FDG, mean (range)	312 (231 – 378)	288 (220 – 372)	
^{18}F-FLT, mean (range)	335 (245 – 382)	327 (272 – 356)	